Interlayer coupling and electronic structure of misfit-layered bismuth-based cobaltites

Sho-ichi Takakura,[1] Isamu Yamamoto,[2] Eishi Tanaka,[3] Junpei Azuma,[2] and Makoto Maki[1,*]

[1]*Department of Physics, Saga University, Saga 840-8502, Japan*

[2]*Synchrotron Light Application Center, Saga University, Saga 840-8502, Japan*

[3]*The Ultramicroscopy Research Center, Kyushu University, Fukuoka 819-0395 Japan*

(Received 11 February 2017; revised manuscript received 14 April 2017; published 30 May 2017)

The $[Bi_2M_2O_4]_pCoO_2$ materials (M = Ca, Sr, and Ba) were studied to clarify the effect of the lattice incommensurability on electronic properties using angle-resolved photoemission spectroscopy and transmission electron microscopy (TEM). Results show that the insulating behavior is characterized by a spectral weight for binding energies higher than 2.0 eV. Moreover, the spectral shape is modified as a function of the incident photon energy, demonstrating a close relationship between the electrical properties and interlayer coupling. TEM results show that the effect of the lattice mismatch differs for different misfit parameters p. We therefore conclude that the carrier concentration and the chemical environment at the misfit interface, which depend on the degree of incommensurability, mutually determine the electronic properties of the system.

DOI: 10.1103/PhysRevB.95.195166

I. INTRODUCTION

Misfit-layered compounds have been studied extensively because of their unique electronic properties [1]. Layered bismuth-based cobaltites described by the general formula $[Bi_2M_2O_4]_pCoO_2$ (M = Ca, Sr, and Ba), which consist of hexagonal CoO_2 layers and rocksalt (RS) type slabs [2,3], have recently attracted attention as potential candidates for thermoelectric applications [4–7]. Their properties depend on the misfit parameter (the b-axis ratio between the CoO_2 and RS structures) p, suggesting that such characteristics are closely related to the incommensurability between those two substructures. Nevertheless, the relevant details remain unclear.

To elucidate the effects of lattice mismatch, we devote particular attention to the temperature-dependent transport behavior [8–11]. The in-plane resistivity ρ_{ab} of $[Bi_2Sr_2O_4]_pCoO_2$ (BSCO) varies considerably with temperature: It exhibits metallic behavior ($d\rho/dT > 0$) at high temperatures, whereas it increases concomitantly with decreasing temperature. The Hall coefficient measurement indicates that the carrier concentration is temperature dependent as well [11]. A similar but more highly insulating trend is found in another member of the misfit-layered cobalt oxide $[Bi_2Ca_2O_4]_pCoO_2$ (BCCO), in which the p value is larger than that of BSCO. For a commensurate system $[Bi_2Ba_2O_4]_{0.50}CoO_2$ (BBCO), in which p is a rational number, ρ_{ab} increases monotonically with temperature. Nonetheless, ρ_{ab} is large and exceeds the so-called Mott-Ioffe-Regel criterion, suggesting an innate similarity among the bismuth-based cobaltites in spite of the different values of p.

Our earlier studies on BSCO have shown that an unusual temperature dependence arises from a change in the local atomic arrangement via scanning tunneling microscopy (STM) and angle-resolved photoemission spectroscopy (ARPES) measurements [12,13]. The rigid band picture is not applicable to BSCO. By changing the temperature, the chemical environment around the oxygen atoms is modified. Consequently, the appearance of inequivalent oxygen sites causes an inhomogeneous charge distribution and loses its spectral intensity near the Fermi level. Now, the remaining issue is how such a phenomenon relates to the structural incommensurability.

As described in this paper, we first compare the ARPES spectra among bismuth-based cobaltites of three kinds. At low temperature, BSCO has a similar high-energy electronic structure to that of BCCO. With increasing temperature, the spectra of BSCO are modified gradually. They become similar to those of BBCO. Therefore, we can deduce that the localization properties are characterized by the evolution of this spectral feature. Then, to investigate the vertical coupling at the misfit interface, we performed ARPES experiments on BSCO with tunable-energy photons using the advantage of synchrotron radiation. Despite the lack of long-range coherence, the temperature-sensitive band structure is dependent on the photon energy, which shows a relationship existing between the anomalous temperature sensitivity and the interlayer bonding, and which gives direct evidence for the contribution of lattice mismatch to the electronic properties. Actually, the effect of the lattice mismatch is neither unidirectional nor uniformly distributed in space. For this study, we visualize the actual atomic arrangement using transmission electron microscopy (TEM) and discuss the structural flexibility of the misfit-layered cobaltites.

II. EXPERIMENTS

Single crystals of bismuth-based cobaltites were grown in Al_2O_3 crucibles using a self-flux method. Details of the growth procedure and x-ray characterization of the samples have been presented previously [12,14]. ARPES measurements were conducted using synchrotron radiation at the Saga University beamline BL13 in the SAGA Light Source [13]. Because of weak van der Waals bonds between the BiO layers, the BiO-terminated surface is clean and stable. To obtain clean surfaces, the single crystals were cleaved *in situ* before the ARPES measurements. Transmission electron microscope (TEM) measurements were conducted on a JEM-3200FSK (JEOL Ltd.) at Kyushu University using an accelerating voltage of 300 kV. Misfit parameters estimated from the

*mmaki@cc.saga-u.ac.jp

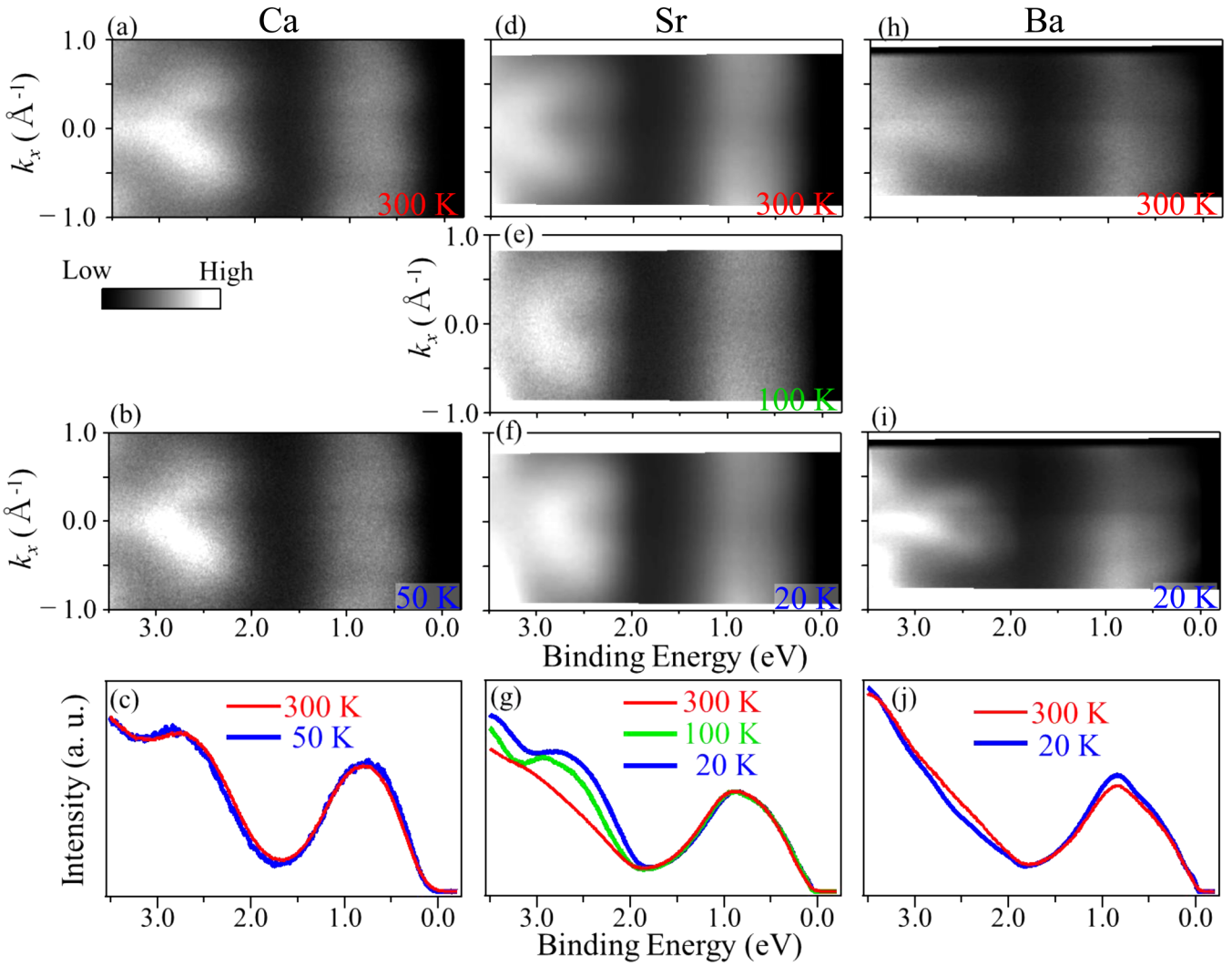

FIG. 1. ARPES intensity plots as a function of energy and wave vector along the ΓM direction of (a), (b) BCCO, (d)–(f) BSCO, and (h), (i) BBCO at various temperatures. The corresponding intensity profiles integrated from $k_x = -1$ to 1 Å^{-1} are shown respectively in (c), (g), and (j) for BCCO, BSCO, and BBCO.

diffraction patterns were $p = 0.51$ and $p = 0.59$, respectively, for BSCO and BCCO.

III. RESULTS AND DISCUSSION

Figures 1(a) and 1(b) respectively portray raw ARPES intensity maps of BCCO obtained at 300 and 50 K. The plot is along the high-symmetry ΓM direction in the two-dimensional hexagonal Brillouin zone (BZ) of the CoO_2 layer. The measurements were conducted using synchrotron radiation with a photon energy of 100 eV. The spectra agree with those reported previously [15], and two valence bands are readily visible: one centered around the binding energy of ∼0.8 eV and another one extended above about 2.0 eV. Figure 1(c) portrays the corresponding intensity profile integrated over the measured k_x range. In fact, the valence band structure of BCCO is independent of temperature, which contrasts to the tendency of BSCO in spite of the similarities in their crystallographic structures [13]. Figures 1(d)–1(f) present raw ARPES intensity maps of BSCO at three temperatures of 300 K [Fig. 1(d)], 100 K [Fig. 1(e)], and 20 K [Fig. 1(f)]. The band structure above 2.0 eV is modified gradually using a change in temperature, as shown clearly in the integrated intensity profile [Fig. 1(g)]. However, the electronic states around ∼0.8 eV are unaffected much. These results mean that changes in temperature induce changes in the local bonding environment. A comparison of Fig. 1(c) with Fig. 1(g) shows that the spectral shape of BCCO closely resembles that of BSCO at 20 K. Figures 1(h)–1(j) portray the case of BBCO having commensurate matching between the CoO_2 and RS structures. As depicted in Fig. 1(j) [16–18], the spectral weight between 2.0 and 3.0 eV, which corresponds to the striking feature of the BCCO spectrum and that of BSCO at 20 K, is suppressed in BBCO. Such a tendency is also observed in the 300 K spectrum of BSCO. As the temperature increases, the band structure of BSCO becomes close to that of BBCO. Therefore, we infer that the spectral structure in the energy region of 2.0–3.0 eV is related to the insulating characteristics of the system.

To elucidate the effects of the structural incommensurability on the electronic structure of the system, we measured the ARPES spectra of BSCO at various photon energies. During photoemission, the wave vector perpendicular to the sample

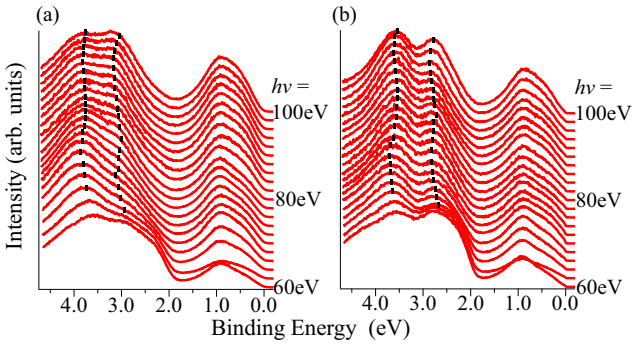

FIG. 2. Energy distribution curves of BSCO as a function of photon energy measured at normal emission with an angle resolution of 0.8°. (a) 300 K and (b) 20 K.

surface is not conserved because of the discontinuity of the potential at the sample surface. However, by assuming a free electron dispersion for the photoelectron final states, the bottom of which has an offset from the vacuum (the inner potential), one can infer a band structure perpendicular to the surface by scanning the photon energy [19]. Figure 2(a) presents the energy distribution curves at the Γ point measured at 300 K with various photon energies from $h\nu = 60$ to 100 eV. At first glance, we notice a broad and slightly dispersive feature centered at about 0.8 eV [20]. However, the band structure in the energy region higher than 2.0 eV is dispersive. This band corresponds to that in which the temperature-driven spectral shift is observed [see Figs. 1(d)–1(f)]. Figure 2(b) presents results for the same sample measured at 20 K. Actually, in comparison to Figs. 2(a) and 2(b), we confirm that the spectral shape varies with temperature.

The corresponding intensity maps in the binding energy range of 2.0–4.6 eV are shown as a function of photon energy in Figs. 3(a) (300 K) and 3(b) (20 K). The same color scale is used for both images. It is readily apparent that

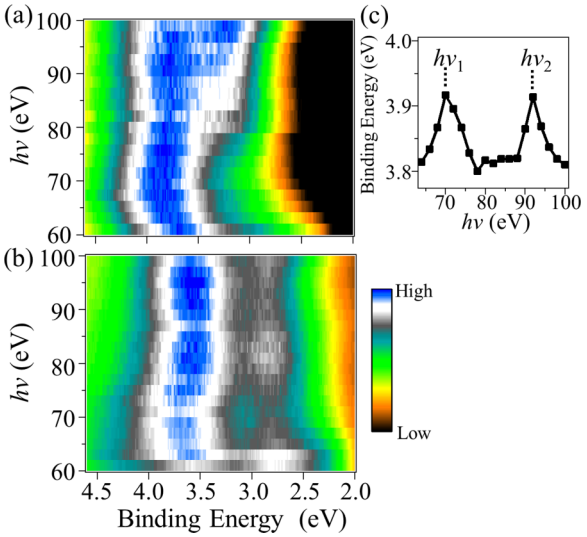

FIG. 3. Intensity maps of the ARPES spectra presented in Fig. 2 at (a) 300 K and (b) 20 K. (c) The positions of spectral peaks in the binding energy region between 3.5 and 4.0 eV in Fig. 2(a).

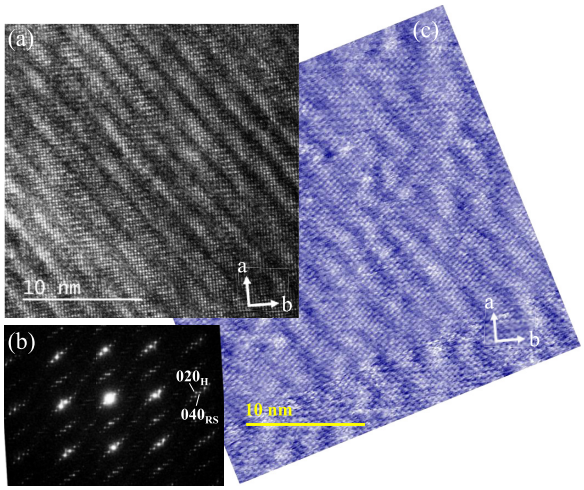

FIG. 4. (a) High-resolution TEM image of the (001) plane of BSCO measured at room temperature. (b) Corresponding diffraction pattern. (c) Constant-height STM image of BSCO taken at $V_{\text{sample}} = -5$ mV and $I = 15$ pA.

the valence band dispersions are modified as the temperature changes. Moreover, it appears that the change in shape of the energy distribution curves exhibits a periodic dependence on the photon energy. The most commonly accepted view is that photoemission spectra at various photon energies probe different $k_\perp$ regions and that they therefore reflect the band dispersion along the c axis [19]. The periodic behavior indicates that multiple Brillouin zones are covered in the energy range. However, those results are rather strange for the following reasons. First, along the c axis, the bonding is expected to be weak because of the misfit. Therefore, the large transfer energy is apparently unlikely. Second, in comparison with Figs. 3(a) and 3(b), we note that the periodic length is varied. Based on the standard interpretation, the result implies that the lattice constant of the c direction is modified considerably by temperature. Finally, the periodic length does not provide a reasonable physical description. Figure 3(c) plots the positions of spectral peaks in the binding energy region between 3.5 and 4.0 eV in Fig. 2(a). For example, a period between approximately $h\nu_1 = 70$ eV and $h\nu_2 = 92$ eV yields a much shorter c length of 10 Å, by assuming a typical order of magnitude of 10 eV for the inner potential [21–25].

The observations demonstrate that the electronic structure is not perfectly two dimensional. The finite charge transfer along the c direction varies with temperature, indicating that the atomic bonding configuration has a close relationship with the lattice mismatch between the two substructures. However, the dispersive features cannot be understood within the framework of conventional $k_\perp$ dispersion. Therefore, we present TEM images, which provide insight into how the lattice mismatch affects the interlayer electronic structure. Figure 4(a) presents a high-resolution TEM image of the (001) plane of BSCO measured at room temperature. The image results from interference of the diffracted beams from the periodic potential of the crystal. The corresponding diffraction pattern is shown in Fig. 4(b), which shows good agreement with the previous results [8,26]. In Fig. 4(a), both the underlying atomic lattice

and the short-range corrugations are clearly visible. The TEM image reflects the projection of atoms aligned in columns along the beam direction. The image contrast is greater for larger atomic numbers. Therefore, the lattice is regarded as consisting of bismuth atoms at and below the surface. This observation is consistent with previously reported STM results [Fig. 4(c)] [12], although the STM image includes only one type of atom in the topmost BiO layer. Good consistency between the TEM and STM images demonstrates that the corrugated pattern extends over the crystal and affects the electronic properties. Furthermore, the TEM measurement provides a clear interpretation for the origin of the corrugated pattern. In dark regions where atomic images are invisible, atoms do not arrange themselves in a regular row. Therefore, it is readily apparent that the crystal structure is divided into multiple microscopic domains, some of which are ordered, although others are not. The existence of the short-range ordered domains implies that the energy gain resulting from the overlapping of atomic orbitals along the *c* axis, even if it is partial, overcomes the energy loss because of the lattice distortion. The TEM image is a projection of the sample. Therefore, ordered regions are expected to be present along the perpendicular direction. Consequently, coherent charge transport and incoherent charge transport coexist along the interlayer direction, which engenders imperfect periodicity of the dispersion map.

Such domain formation is not necessary for all the misfit-layered cobaltites. Figure 5 portrays a TEM image of BCCO at room temperature, together with the corresponding diffraction pattern (inset). Actually, a clear sign of domain formation cannot be found, although the atomic images are somewhat less sharp. The observations were reproducible within and between samples. We reported previously that the lattice deformation in BSCO depends on the temperature [12]. The present results suggest strongly that the structural flexibility is related to the existence of ordered domains connected by disordered linkers. The lattice mismatch expected from the ionic radius is about 6.2% between the BiO and SrO layers and about 1.3% between the BiO and CaO layers [27], which indicates that the lattice strain in the RS slab of BSCO is slightly greater than that of BCCO, although compressive (tensile) stresses act in the opposite direction. Moreover, it is expected that the carrier concentration plays an important role in domain formation: When the carrier density increases, a greater energy gain is obtained by orbital mixing along the *c* direction. When insufficient energy is available, the domain structure is not formed. The bonding configuration is fine tuned to avoid the energy loss caused by the lattice mismatch. We infer that this is the case for BCCO. Therefore, the structural incommensurability leads not only to the carrier generation but also to inhomogeneous local deformations, both of which are combined to determine the electronic properties of the system.

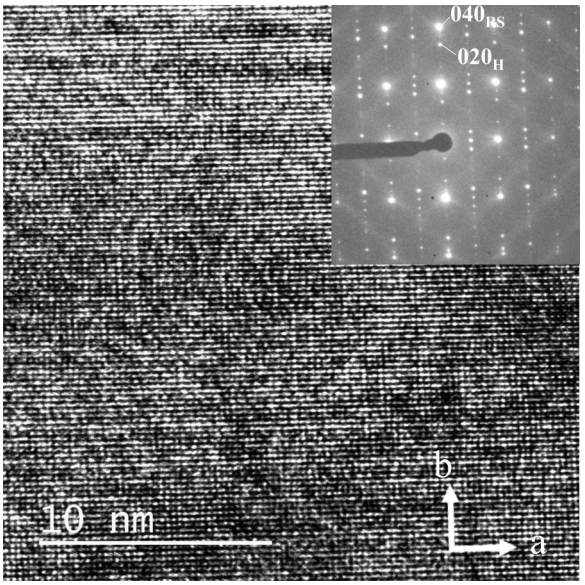

FIG. 5. High-resolution TEM image of the (001) plane of BCCO measured at room temperature. The corresponding diffraction pattern is shown in the inset.

IV. CONCLUSIONS

In conclusion, using ARPES and TEM we investigated the effect of structural incommensurability on the electronic structure of layered bismuth-based cobaltites. We have shown that the high-energy electronic structure of BSCO resembles that of BCCO at low temperature but becomes similar to that of BBCO at high temperature. This temperature-sensitive band structure reveals the incident photon energy dependence, demonstrating a close relationship between the electrical properties and the interlayer coupling. However, the out-of-plane momentum dependence of the band dispersion is imperfect, which is probably attributable to the microscopic domain formation shown by the TEM micrograph. No similar domain structure has been found in BCCO. Therefore, we conclude that the carrier concentration and the amount of strain, both of which are controlled by the degree of lattice mismatch, cooperatively determine the electronic structure of the misfit-layered bismuth-based cobaltites.

ACKNOWLEDGMENTS

This work was partly supported by the Advanced Characterization Platform of the Nanotechnology Platform Japan. We are grateful to Y. Tomokiyo of Kyushu University for their helpful support for transmission electron microscopy analysis.

[1] G. A. Wiegers, Prog. Solid State Chem. **24**, 1 (1996).
[2] M. Hervieu, Ph. Boullay, C. Michel, A. Maignan, and B. Raveau, J. Solid State Chem. **142**, 305 (1999).
[3] H. Leligny, D. Grebille, O. Pérez, A. C. Masset, M. Hervieu, and B. Raveau, Acta Crystallogr., Sect. B **56**, 173 (2000).

[4] R. Funahashi, I. Matsubara, and S. Sodeoka, Appl. Phys. Lett. **76**, 2385 (2000).
[5] T. Itoh and I. Terasaki, Jpn. J. Appl. Phys. **39**, 6658 (2000).
[6] A. Maignan, W. Kobayashi, S. Hébert, G. Martinet, D. Pelloquin, N. Bellido, and Ch. Simon, Inorg. Chem. **47**, 8553 (2008).
[7] J. D. Baran, D. Kepaptsoglou, M. Molinari, N. Kulwongwit, F. Azough, R. Freer, Q. M. Ramasse, and S. C. Parker, Chem. Mater. **28**, 7470 (2016).
[8] J.-M. Tarascon, R. Ramesh, P. Barboux, M. S. Hedge, G. W. Hull, L. H. Greene, M. Giroud, Y. LePage, W. R. McKinnon, J. V. Waszcak, and L. F. Schneemeyer, Solid State Commun. **71**, 663 (1989).
[9] A. Maignan, S. Hébert, M. Hervieu, C. Michel, D. Pelloquin, and D. Khomskii, J. Phys.: Condens. Matter **15**, 2711 (2003).
[10] M. Hervieu, A. Maignan, C. Michel, V. Hardy, N. Créon, and B. Raveau, Phys. Rev. B **67**, 045112 (2003).
[11] S. Hébert, W. Kobayashi, H. Muguerra, Y. Bréard, N. Raghavendra, F. Gascoin, E. Guilmeau, and A. Maignan, Phys. Status Solidi A **210**, 69 (2013).
[12] M. Maki, S.-i. Takakura, T. Nishizaki, and F. Ichikawa, Phys. Rev. B **92**, 165117 (2015).
[13] S.-i. Takakura, I. Yamamoto, E. Koga, F. Ichikawa, J. Azuma, and M. Maki, Phys. Rev. B **93**, 165118 (2016).
[14] M. Maki, K.-i. Machida, T. Mori, T. Nishizaki, and N. Kobayashi, Phys. Rev. B **78**, 073101 (2008).
[15] V. Brouet, A. Nicolaou, M. Zacchigna, A. Tejeda, L. Patthey, S. Hebert, W. Kobayashi, H. Muguerra, and D. Grebille, Phys. Rev. B **76**, 100403(R) (2007).
[16] As reported previously, a quasiparticle peak appears just below the Fermi level in BBCO, which is smeared in Fig. 1(j) due to the integration over the momentum space.
[17] Z. Yusof, B. O. Wells, T. Valla, P. D. Johnson, A. V. Fedorov, Q. Li, S. M. Loureiro, and R. J. Cava, Phys. Rev. B **76**, 165115 (2007).
[18] A. Nicolaou, V. Brouet, M. Zacchigna, I. Vobornik, A. Tejeda, A. Taleb-Ibrahimi, P. Le Févre, F. Bertran, S. Hébert, H. Muguerra, and D. Grebille, Phys. Rev. Lett. **104**, 056403 (2010).
[19] F. J. Himpsel, Adv. Phys. **32**, 1 (1983).
[20] Near the $3p$ absorption edges of Co ($\sim$60 eV), the resonant signal is superimposed on the spectra.
[21] A. R. Law, M. T. Johnson, and H. P. Hughes, Phys. Rev. B **34**, 4289 (1986).
[22] D. L. Feng, C. Kim, H. Eisaki, D. H. Lu, A. Damascelli, K. M. Shen, F. Ronning, N. P. Armitage, N. Kaneko, M. Greven, J.-i. Shimoyama, K. Kishio, R. Yoshizaki, G. D. Gu, and Z.-X. Shen, Phys. Rev. B **65**, 220501(R) (2002).
[23] T. Sato, K. Terashima, S. Souma, H. Matsui, T. Takahashi, H. Yang, S. Wang, H. Ding, N. Maeda, and K. Hayashi, J. Phys. Soc. Jpn. **73**, 3331 (2004).
[24] S. Basak, T. Das, H. Lin, J. Nieminen, M. Lindroos, R. S. Markiewicz, and A. Bansil, Phys. Rev. B **80**, 214520 (2009).
[25] T. Arakane, T. Sato, T. Takahashi, T. Fujii, and A. Asamitsu, Phys. Rev. B **81**, 115132 (2010).
[26] K. Yubuta, S. Begum, Y. Ono, Y. Miyazaki, and T. Kajitani, Jpn. J. Appl. Phys. **45**, 4159 (2006).
[27] R. D. Shannon, Acta Crystallogr., Sect. A **32**, 751 (1976).